

Orchestrating Asymmetric Surface Functionalities on Hydrogel Stamps where Adhesion Meets Lubrication

Mingfei Pan, Tao Shui, Ziqian Zhao, Mei Li, Hongbing Fan, Jianping Wu, and Hongbo Zeng*



Cite This: <https://doi.org/10.1021/acs.chemmater.3c00347>



Read Online

ACCESS |



Metrics & More

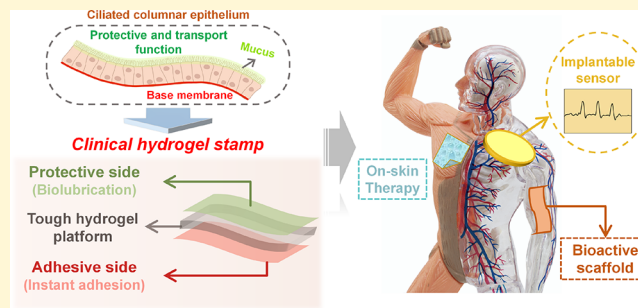


Article Recommendations



Supporting Information

ABSTRACT: Bioadhesives applied on human organs are promising soft implants for interventional diagnostics and therapeutics. However, the conventional bioadhesive interfaces on organs typically lack apical–basal polarity to resemble the surface functions of original organ epithelia. To overcome the bioadhesive-induced dysfunction on treated organs, we have developed an innovative strategy via engineering asymmetric surface functionalities on a tough yet biodegradable polysaccharide-peptide-derived hydrogel platform, mimicking the functions of a ciliated columnar epithelium enabled by its adhesive basal surface and defensive apical ciliated surface. The resulting hydrogel bioadhesive serves as a “stamp” with a polyacrylic acid-functionalized adhesive side, facilitating instant and robust adhesion on wet tissues within 1 min via body liquid-removing mechanisms and Ca^{2+} -assisted complexation. The back side is functionalized with hyaluronic acid, demonstrating an outstanding biolubrication performance (coefficient of friction of ~ 0.038 in the synovial fluid). The hydrogel stamp can also be integrated with biosensing and drug encapsulation/release functions for diagnostics and therapeutics. Our strategy devises a new path to simultaneously enable reliable wet tissue adhesion and reproduce the characteristics of original tissues, with useful insights into designing bioactive interfaces for broad biomedical applications.



tissues within 1 min via body liquid-removing mechanisms and Ca^{2+} -assisted complexation. The back side is functionalized with hyaluronic acid, demonstrating an outstanding biolubrication performance (coefficient of friction of ~ 0.038 in the synovial fluid). The hydrogel stamp can also be integrated with biosensing and drug encapsulation/release functions for diagnostics and therapeutics. Our strategy devises a new path to simultaneously enable reliable wet tissue adhesion and reproduce the characteristics of original tissues, with useful insights into designing bioactive interfaces for broad biomedical applications.

INTRODUCTION

The innovation of medical techniques for diagnosis and treatment has posed a considerable challenge: developing advanced biomaterials to enable stable fixation and high-efficient interfacing with soft tissues. Traditional fixation methods in physiological environments using sutures and staples entail experienced surgical operations and are time-consuming.^{1–3} Meanwhile, these metal-based materials are mechanically mismatched with soft tissues and inevitably bring damage and discomfort to patients.^{4–9} In light of these drawbacks, hydrogel-based bioadhesives have been introduced and explored for decades attributed to their unique features of minimal invasion and simplified surgical procedures. Previous research has focused on the design of interfacial interactions between hydrogel adhesives and target substrates via two major mechanisms, specifically modulating marine mussel-derived catechol chemistry^{10–15} and engineering topological connections^{16,17} at contact interfaces. These hydrogels are mainly double-side adhesives with symmetric surface functions and are designed for applications such as substitutions of connective tissues. However, in practical scenarios, single-side adhesion is more desirable on the epithelium of organs with the basal side binding to the target tissue area and the apical side to reproduce the surface characteristics of original tissues such as lubrication function that can reduce potential tissue damage caused by postoperative adhesion and wears.^{18–21} Integrating functional

layers on the bioadhesives is one of the existing methods to generate single-side adhesives, but their application is still limited by the complicated assembling process of the sandwich-type structure and the insufficient stability among layers. Thus, although great improvement has been achieved in the area of hydrogel-based wet tissue adhesion, developing a highly efficient bioadhesive with asymmetric surface functionalities is of critical significance yet challenging.

Herein, we have developed a new series of tough and bioresorbable hydrogels prepared by crosslinking gelatin and polysaccharides (i.e., carboxymethyl cellulose and chitosan) that can be used as dressing materials. Inspired by the distinct functions of defensive cilia and the adhesive base membrane at opposite sides of the ciliated columnar epithelium (CCE), the hydrogel is then functionalized with asymmetric surface functionalities on its opposite sides and serves as a stamp-like single-side adhesive (Figure 1A). The adhesive side of the hydrogel is coated with a thin layer of polyacrylic acid (PAA) to

Received: February 15, 2023

Revised: June 8, 2023

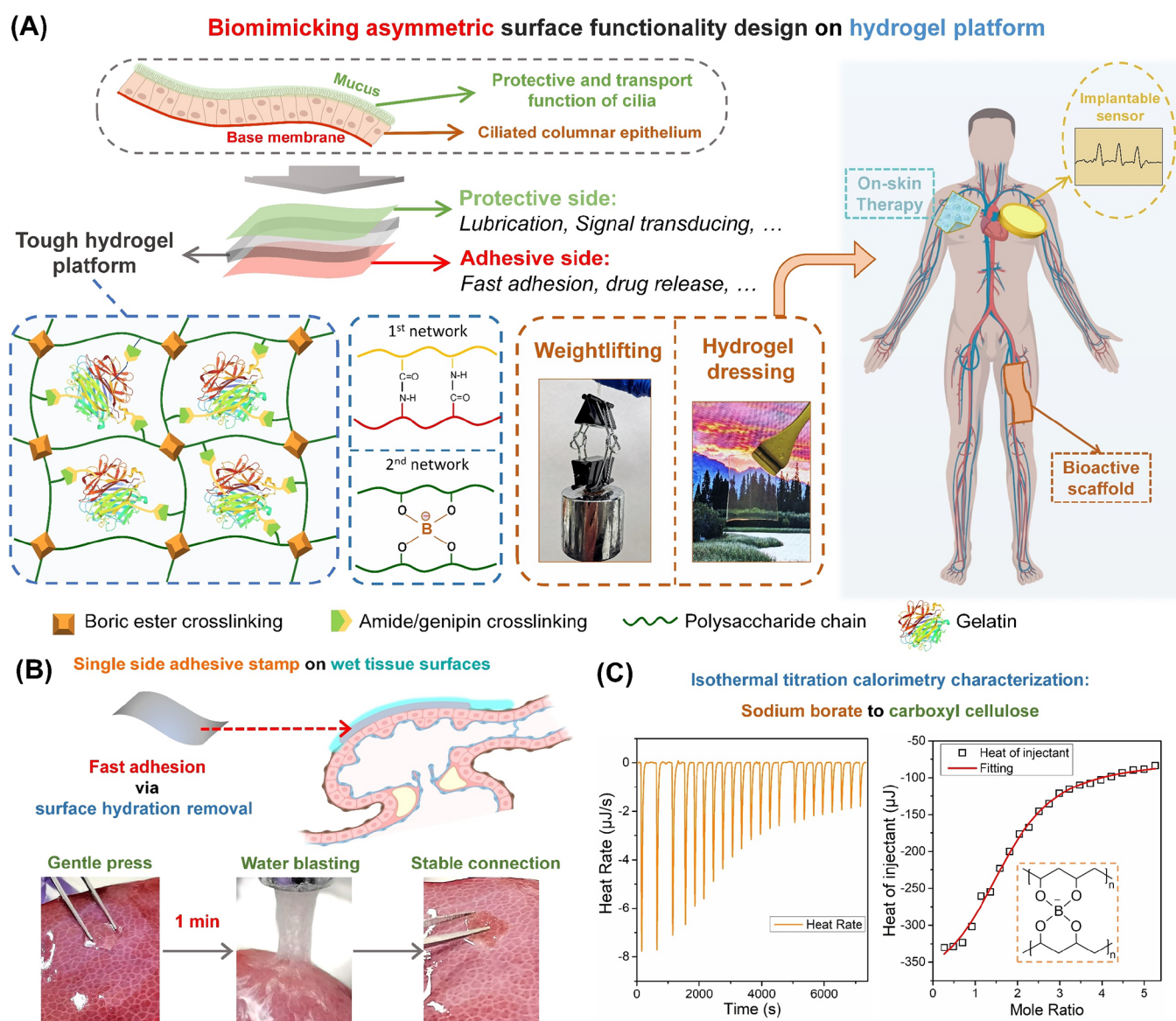


Figure 1. Design of asymmetric surface functionalities on a hydrogel platform. (A) Schematic illustration of the crosslinking strategy for the formation of a tough hydrogel platform and its optical images. (B) Demonstration of the hydrogel stamp with instant and robust adhesion capability on a wet liver surface. (C) Isothermal titration calorimetry characterization of reactions between carboxyl cellulose and sodium borate for boric ester bond-derived hydrogel crosslinking.

facilitate the instant and robust binding with wet substrates (Figure 1B). The adhesion of the hydrogels is ascribed to the synergy of hydrogen bonding and metal complexation adopted from the adhesion chemistry of marine organisms (e.g., *Mytilus edulis* and barnacle).^{5,7,16} The protective side of the hydrogel is coated by a thin layer of hyaluronic acid (one of the key components for wear reduction in a joint system) to enhance the hydration capability for lubrication. The polymer network of the hydrogel is constructed after a 2-step crosslinking strategy with amide and borate ester crosslinking for mechanical reinforcement, which helps resist the high stress from tissue movement.^{22,23} The mechanical performance of the developed hydrogels was characterized by tensile and rheology tests, exhibiting a high elastic modulus and toughness up to 0.8 MPa and 40 MJ/m³, respectively, close to the mechanical property of load-bearing tissues (e.g., tendons). Meanwhile, the hydrogel-based drug release capability for treatment and intelligent sensing functions for diagnosis were also demonstrated, further

broadening its biomedical applications. The cytotoxicity and cell affinity of the developed hydrogels were characterized and confirmed by 2D cell culture experiments with the mouse osteoblast MC3T3-E1. Owing to the precise design of surface functionalities on hydrogels, it was hypothesized that the as-prepared hydrogel stamp well meets the previously overlooked requirements of dressing materials for biological tissues, which holds great promise to be further engineered and utilized in clinical procedures.

RESULTS AND DISCUSSION

Although hydrogels are a common type of soft matter in nature, most of synthetic hydrogels are intrinsically weak in mechanical strength. Developing tough hydrogel materials as the bioactive framework is significant and desirable for a wide range of biomedical applications. In this work, a two-step crosslinking strategy was employed in a polysaccharide-peptide-based network to fabricate the tough hydrogels. The original

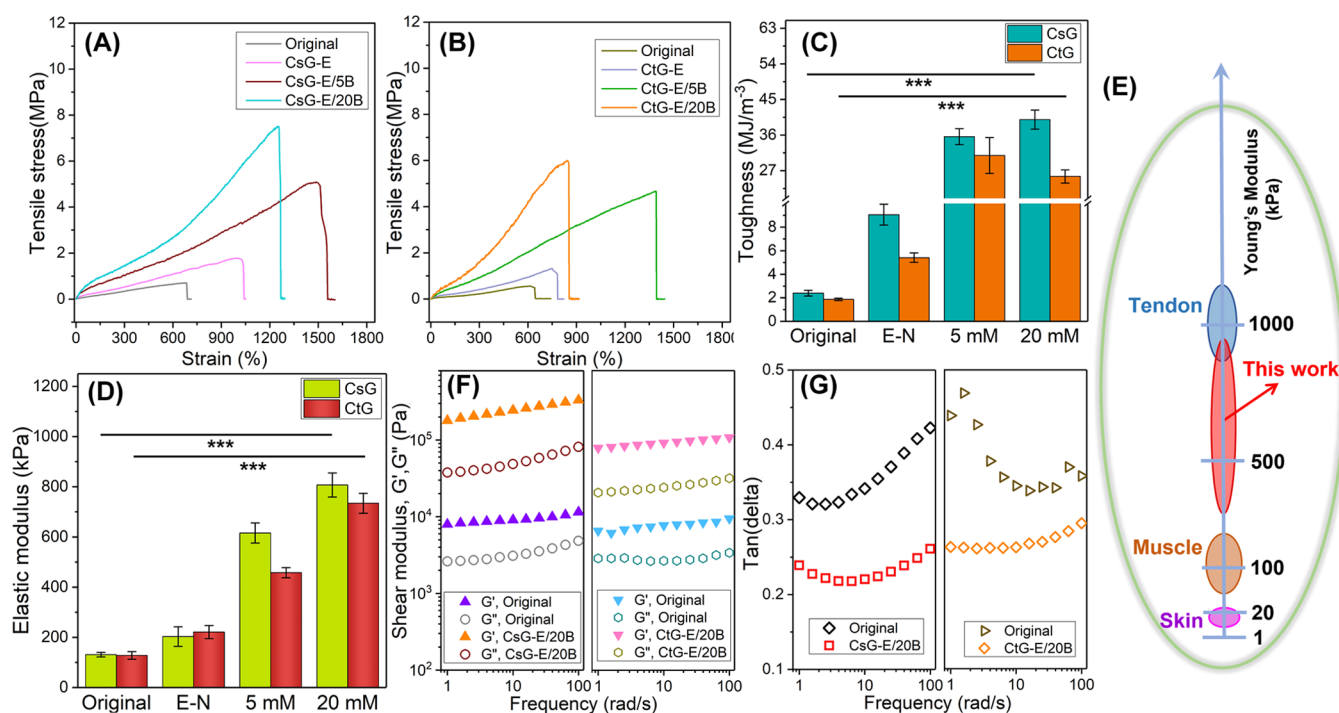


Figure 2. Mechanical properties of the hydrogels. Typical stress–strain curves of (A) CsG and (B) CtG hydrogels; (C) toughness and (D) elastic modulus calculated from the corresponding tensile tests (\pm standard deviation, SD, for $n = 3$ replicates per condition, $***P < 0.001$); (E) modulus range of typical soft tissues in the human body and the developed hydrogels in this work; (F) frequency-dependent rheological measurements (storage modulus G' and loss modulus G'') of CsG and CtG hydrogels with (G) $\tan \delta$ (G''/G').

carboxymethyl cellulose-gelatin (CsG) and chitosan-gelatin (CtG) hydrogels were first crosslinked in the solution of 1-ethyl-3-(3-dimethylaminopropyl)carbodiimide hydrochloride/*N*-hydroxysulfosuccinimide (EDC-NHS) via the formation of amide bonds between carboxyl and amine groups of carboxymethyl cellulose (Cs), chitosan (Ct), and gelatin (G).^{24,25} The obtained CsG-E and CtG-E hydrogels were further treated by sodium borate to form boric ester bonds with polyhydroxy moieties of the hydrogels.^{23,26} The optical images of the hydrogels after two-step crosslinking (denoted as CsG-E/B and CtG-E/B) are shown in Figure S1A. Both the CsG-E/B and CtG-E/B are transparent with the transmittance of ~ 80 –90% and 50–75% within the range of visible light (Figure S1B) characterized by the UV–vis spectrum, which enables the transmission of optical signals within the hydrogels. The morphology of the obtained hydrogels was then characterized by field-emission scanning electron microscopy (FE-SEM) (Figures S2 and S3). Both the CsG-E/B and CtG-E/B hydrogels exhibit a highly porous honeycomb-like structure, suggesting the uniform crosslinking of the hydrogels. The chemical functionality of the developed hydrogels was then characterized using the Fourier-transform infrared (FTIR) spectroscopy, as shown in Figures S3 and S4. To gain insight into the molecular basis of affinity for borate with polysaccharides, isothermal titration calorimetry (ITC) characterization was conducted. As illustrated in Figure 1C, the raw output of an ITC experiment of the heat exchange rate per injection (sodium borate to Cs solution) was calculated to obtain the heat of injection as a function of the molar ratio. The red line shows the fitted results to a binding algorithm from which the enthalpy (ΔH) and entropy (ΔS) of the interaction are determined. For comparison, the titration of sodium borate to gelatin was also conducted (Figure S6). The ΔH of borate/Cs and borate/GI was measured to be -90.7 and

$-40.2 \text{ kJ} \cdot \text{mol}^{-1}$, respectively. The ΔS of borate/Cs and borate/GI was measured to be -199 and $-28.8 \text{ J} \cdot \text{K}^{-1} \cdot \text{mol}^{-1}$, respectively. The higher ΔH of borate/Cs suggests their strong interactions compared to that of borate/GI, which could be attributed to the dense hydroxyl groups of the natural polysaccharides forming boric ester bonds with borates. Meanwhile, the greatly negative ΔS of borate/Cs indicates the significant decrease of system randomness compared to that of borate/GI, implying the crosslinking of Cs in the presence of borates.

The mechanical properties of the obtained hydrogels were then investigated by both the tensile tests and rheological measurement. As shown in Figure 2A, from the tensile stress–strain curves, the fracture strength and strain of the original CsG hydrogel were 0.70 MPa and 670%, while those of the CsG-E hydrogel after EDC/NHS treatment were increased to 1.7 MPa and 990%, demonstrating an effective mechanical enhancement to the original CsG hydrogel. A similar trend was also observed in the tensile stress–strain curves (Figure 2B) of the CtG-E hydrogel with a 140% increase in fracture strength and a 22% increase in fracture strain compared to the original CtG hydrogel. Compared to the original CsG and CtG hydrogels that are physically assembled by hydrogen bonding and electrostatic interactions, the CsG-E and CtG-E hydrogels are chemically crosslinked by forming amide bonds between the carboxyl and amine groups of CS, CT, and GL. After that, sodium borate solution was used to treat the CsG-E and CtG-E hydrogels. As shown in Figure 2A, introducing 5 mM sodium borate resulted in a 200% increment in tensile strength of the obtained CsG-E/SB hydrogel, reaching 5.1 MPa and 1500% for fracture strength and strain, respectively. Further increasing the concentration of sodium borate to 20 mM, the fracture strength of CsG-E/20B raised slightly to 7.5 MPa, while its stretchability

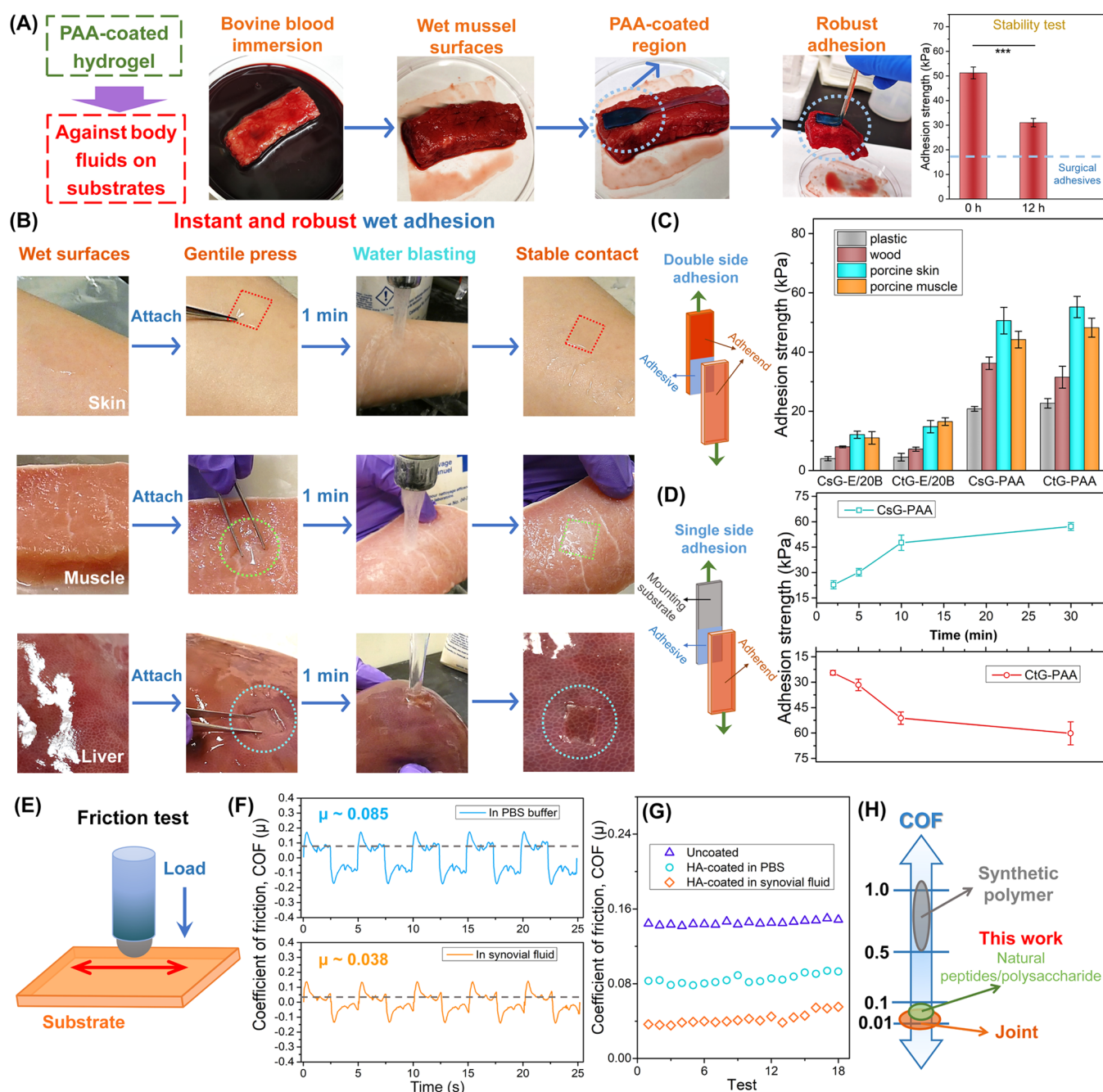


Figure 3. Adhesion and lubrication properties of the hydrogels. (A) Optical images showing the adhesion performance of a partially PAA-coated hydrogel stamp on bovine blood-enriched tissue surfaces with stability tests (\pm SD for $n = 4$ replicates per condition, $***P < 0.001$). (B) Instant adhesion property of the CsG hydrogel stamp on different wet tissues. (C) Adhesion strength of CsG and CtG hydrogels on different wet substrates (\pm SD for $n = 3$ replicates per condition); (D) effect of attaching time to the adhesion property of the hydrogels (\pm SD for $n = 3$ replicates per condition). (E) Experimental setup of the NTR³ nanotribometer for conducting reciprocating ball-on-disk friction tests; (F) COF versus time curves measured on CsG hydrogels in PBS buffer and synovial fluids; (G) COF variation at the sliding stage within 20 tests; (H) COF of conventional synthetic polymers and the human joint.

was restricted with a fracture strain of 1250%. A similar effect of tensile strength enhancement with sodium borate was also observed in CtG hydrogels (Figure 2B). Sodium borate is a natural buffer solution, and even a very low concentration of 100 μ M could result in an apparent solution alkalinity (pH > 9). The CsG-E/20B and CtG-E/20B hydrogels were washed 3 times after the treatment, and pH values of the washing solutions were monitored. After the first washing step that removed the freely adsorbed borate ions, the pH of second and third washing

solution decreased to around 7.2 for both the CsG-E/20B and CtG-E/20B hydrogels (Figure S7), indicating the stability of boric ester bonds after their reaction that cannot be released in an aqueous environment.

The toughness and elastic modulus of the CsG and CtG hydrogels were then calculated accordingly and are illustrated in Figure 2C,D. After the two-step crosslinking, the toughness of original CsG and CtG hydrogels increased significantly (from 0.205 to 41.3 MJ/m³ for carboxymethyl cellulose-based ones

and 0.212 to 26.5 MJ/m³ for chitosan-based ones), which surpass most of the natural biopolymer-based hydrogels^{27–29} and ensure their durability as the hydrogel platform for the postmodification and potential applications. Meanwhile, the effect of amide and boric ester crosslinking could also be observed from the variation of the elastic modulus for both CsG (from 123 to 815 kPa) and CtG (from 112 to 648 kPa) hydrogels, enabling a mechanical match with the human tissues (e.g., skin, muscle, and organs) (Figure 2E). To further investigate the network structure of the developed hydrogels, rheological measurement was applied to characterize their viscoelastic behaviors. Figure 2F shows the storage modulus G' and loss modulus G'' of CsG-E/20B and CtG-E/20B hydrogels at angular frequencies ranging from 1 to 100 rad/s. Both hydrogels exhibited a solid-like behavior ($G' > G''$) across the frequency range. Additionally, the storage and loss moduli greatly increased after the two-step crosslinking process. Meanwhile, CsG-E/20B and CtG-E/20B possessed lower $\tan \delta$ values (G''/G') at low to high frequencies (1–100 rad/s) compared to original CsG and CtG (Figure 2G), respectively. This result suggests the successful formation of a more elastic carboxymethyl cellulose/chitosan-gelatin network after crosslinking. The results from the rheological measurement also provide an insightful explanation of the tensile test results that the covalent bond formed between the polymer network altered the viscoelastic behaviors of the hydrogel and induced a significant enhancement in the elasticity, resulting in the effective mechanical reinforcement of the hydrogel.

At the side facing the target substrates, the CsG-E/20B and CtG-E/20B hydrogels were surface functionalized by a layer of PAA coating (denoted as CsG-PAA and CtG-PAA) to enable the adhesion property. The chemical functionality and wetting property on the surface of the hydrogel were characterized by FTIR spectroscopy (Figures S4 and S5) and water contact angle (WCA) measurement in air (Figure S9), respectively. Introducing PAA on the hydrogel surface resulted in an increased hydrophilicity (WCA from $\sim 20^\circ$ for the uncoated ones to $\sim 2^\circ$ for the coated ones), which enhanced the hydration capability of the hydrogels for the body fluid-removing functions during the wet adhesion process.³⁰ As shown in Figure 3A, the CsG-E/20B hydrogel was partially coated with PAA (also dyed by Basic Blue) and attached to the porcine muscle surfaces that were pretreated in bovine blood. A drop of CaCl₂ solution (20 mM) was also spread on the target area. After 10 min of gentle pressing, only the coated region established a stable connection with the substrate to lift the attached porcine muscle. The stable adhesion could be sustained in a wet environment (citrated bovine blood) for 12 h with a 38% reduction in adhesion strength. Despite this reduction, the adhesion strength remains significantly higher than that of existing surgical biogluue (as shown in Figure 3A).³¹ In practical scenarios, the adhesion formation of hydrogels on wet substrates is typically time-consuming due to the appearance of surface hydration. However, in this work, the PAA-coated hydrogel stamp at its dry state could rapidly adsorb the surface fluids to enable an intimate contact with the substrates to promote the formation of an intimate interfacial adhesion.^{5,31–33} This design addresses the long-standing challenge faced by hydrogel-based adhesives, which typically exhibit reduced performance on wet biological tissues. The developed hydrogel stamps were then applied on different wet substrates, as illustrated in Figure 3B and Videos S1–S3. After a gentle press, the hydrogel stamp could instantly attach to the substrates (i.e., the skin, muscle, and liver) and

form a stable connection within 1 min. The hydrogel stamps could resist water blasting, which demonstrated the great stability of their adhesion with substrates. The adhesion strength of the hydrogel stamp was characterized by lap-shear tests on diverse substrates including plastic, wood, porcine skin, and bovine muscle (force–distance curves in Figure S10). As shown in Figure 3C, the adhesion strength of PAA-coated CsG-E/20B and CtG-E/20B hydrogels is significantly increased compared to uncoated ones. For instance, after a 20 min contact, the adhesion strengths of bare CsG-E/20B and CtG-E/20B hydrogels on porcine skin are 14.1 and 14.8 kPa, respectively, while those of CsG-PAA and CtG-PAA hydrogels are 50.6 and 55.2 kPa, respectively. The enhanced adhesion strength is mainly due to the PAA coating on the hydrogel surface and Ca²⁺ in the solution generating interfacial bonding (hydrogen bonding and Ca²⁺ complexation) to strengthen the connection between the hydrogel surfaces and target substrates.^{34,35} Meanwhile, the performance of the hydrogel stamp also depends on the contact time. Single-side adhesion tests were conducted to simulate the use of the hydrogel stamp with varied contact time. As shown in Figure 3D, a rapid increase of the adhesion strength for CsG-PAA and CtG-PAA hydrogels was observed at the first 10 min of the contact time. Further increasing the contact time did not greatly intensify the performance of the developed stamps. To summarize, the obtained hydrogel stamps demonstrate an instant and stable adhesion performance, which is superior to most of the commercial bioglues such as fibrin-glue TISSEEL and collagen-based sealants with the adhesion strength typically below 20 kPa.³⁶

The lubrication side of CsG-E/20B and CtG-E/20B hydrogels is surface-functionalized with HA coating (denoted as CsG-HA and CtG-HA) to generate a slippery surface for wear reduction. The wetting property on the lubrication side of the hydrogel was characterized by WCA measurement in air (Figure S9). Compared to the bare CsG-E/20B and CtG-E/20B hydrogels with the WCA of $\sim 20^\circ$, the WCA on CsG-HA and CtG-HA was close to 0° with a rapid spreading process of less than 1 s, which could be explained by the hydration capability of HA molecules on hydrogel surfaces. The frictional property of the CsG-HA hydrogel was then evaluated by conducting the reciprocating ball-on-disk friction test using an NTR³ nanotribometer (Figure 3E). In a typical friction test cycle, the stiction stage followed by dynamic sliding stage could be observed (Figure S11). The coefficient of friction (COF) was calculated from the shear forces at the sliding stage and normal loading. Figure 3F,G shows the COF of CsG-HA measured in different fluids (i.e., the PBS solution and synovial fluid). The COF of the CsG-HA hydrogel in PBS buffer was ~ 0.085 , which was only half of that with the bare CsG-E/20B hydrogel, demonstrating the lubrication effect of HA coating on the hydrogel surface. Meanwhile, the COF of the CsG-HA hydrogel was further decreased in the synovial fluid, reaching ~ 0.038 . This could be attributed to the function of the synovial fluid containing hyaluronan and lubricin to protect the hydrogel substrate. The results from the friction tests demonstrate the superior lubrication performance of the CsG-HA hydrogel in the simulated biological environment, approaching the performance in the human joint (Figure 3H).³⁷

The biocompatibility of the developed hydrogels was investigated by 2D culture of mouse osteoblast MC3T3-E1 cells. Cells cultured without hydrogels were set as a control. Evaluated by the MTT assay, CsG-E/20B and CtG-E/20B hydrogels exhibited no obvious cell toxicity, and >95% viability

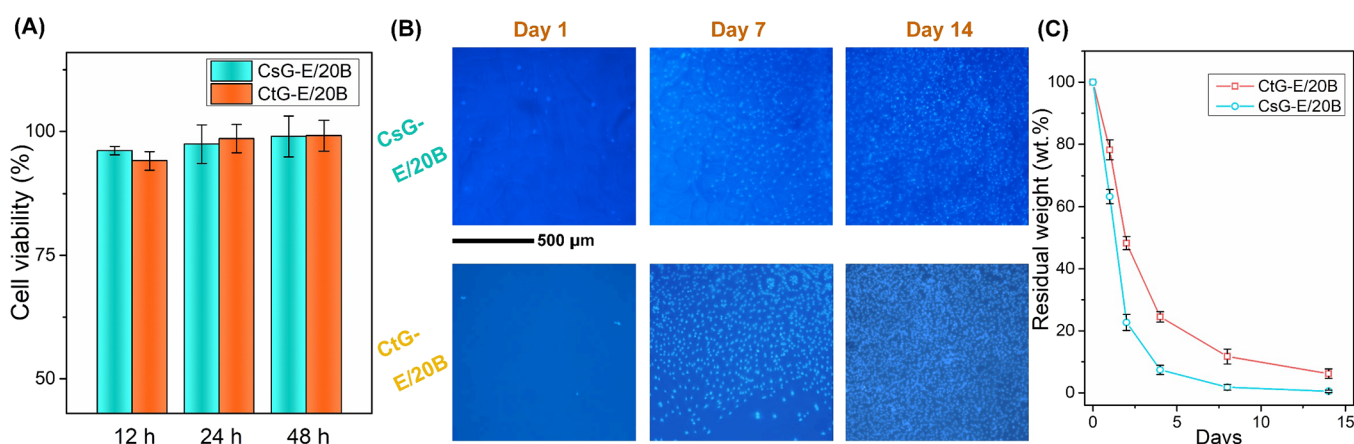


Figure 4. Biocompatibility and biodegradability of the hydrogels. (A) Viability of MC3T3-E1 cells after 12, 24, and 48 h of incubation with CsG-E/20B and CtG-E/20B hydrogels (\pm SD for $n = 3$ replicates per condition, $p > 0.05$); (B) fluorescence microscopy images showing cell proliferation on hydrogels surfaces after 14 days (scale bar, 500 μ m). (C) Degradation tests of CsG-E/20B and CtG-E/20B hydrogels in PBS buffer containing 1 mg/mL collagenase and lysosomes (\pm SD for $n = 3$ replicates per condition).

was maintained within 48 h of incubation (Figure 4A). To further investigate the interaction of the developed hydrogels with MC3T3-E1 cells, fluorescence microscopy was employed to visualize the proliferation of MC3T3-E1 cells grown inside the hydrogel via dyeing the nuclei with 4',6-diamidino-2-phenylindol (DAPI). As shown in Figure 4B, cells were proliferated rapidly and significantly on both the CsG-E/20B and CtG-E/20B hydrogels from day 1 to 14. As a comparison, fluorescence microscopy was also applied to the classic PVA hydrogel used as implantable materials from the previous research. No cell attachment and proliferation were observed on PVA hydrogels (Figure S12). This is due to the gelatin moieties in the hydrogels that contain the arginine–glycine–aspartic acid (RGD) sequence, which is essential for cell adhesion through interactions with integrin.^{38,39} Meanwhile, the developed hydrogels in this work were all made from natural gelatin and polysaccharides that could be degraded by the biological system with the appearance of enzymes.^{31,40–42} The biodegradability test of the hydrogels was conducted in the PBS solution with lysosomes and collagenase A at 37 °C. The residual weight of CsG-E/20B and CtG-E/20B hydrogels was below 10% after 14 days of incubation, which promotes their long-term biosafety as guest materials in biological systems. The fouling of microbes on the soft implants could trigger the undesirable immune response. The antibiofouling performance was evaluated by the bacteria adhesion assay by using *Escherichia coli* (*E. coli*) as the model foulants. As shown in Figure S12, the introduction of HA coating on the CsG hydrogel reduces the *E. coli* coverage from 1.7 to 0.1% after 4 h of incubation. The bacteriostatic activity of the HA coating is ascribed to its antiadhesive property since HA contains no bactericidal effects.⁴³ Interestingly, the *E. coli* coverage on both CtG-E/20B and CtG-E/20B-HA is very low (below 0.1%), which is mainly due to the inhibition effect of chitosan carrying a positive charge interacting with the negatively charged bacterial membrane.⁴⁴ These results indicated the excellent biocompatibility, cell affinity, and antimicrobial property of the developed CsG-E/20B and CtG-E/20B hydrogels, which hold great promise being used as the bioactive scaffold materials.

In addition to the adhesion and lubrication properties, we also investigated the capability of the as-prepared hydrogel stamp for drug encapsulation/delivery, hydration retention, and sensing functions. We first tested the drug release property of this

hydrogel in response to different biological environments. As shown in Figure 5A, using Congo red (CR) as a model drug, the CR-loaded CsG-E/20B hydrogel exhibited a distinct release process in pure and lysosome-containing PBS solution. It could also be observed from the cumulative release curve of CR measured by the UV–vis spectrum, reaching ~20 and 60% release of CR in pure and lysosome-containing PBS solutions after 72 h, respectively. In biological fluids, the existence of different enzymes could induce the degradation of gelatin and polysaccharide moieties in the hydrogel, resulting in a higher amount of drug release.^{45,46} We further investigated the release property of the CsG-E/20B hydrogel loaded with an antioxidant drug (curcumin) and an anti-inflammatory drug (diclofenac). The calculated kinetic constants are summarized in Figure 5C. These three drugs all exhibited a higher release rate in the lysosome-containing environment with the kinetic constants one magnitude higher than that of in pure PBS solution. The interfacial release process was characterized and visualized using a mIRage OPT-IR microscope.⁴⁷ Figure 5D,E shows the IR images of the substrates before and after contact with the drug-loaded hydrogels. The images were scanned at the characteristic peaks of the corresponding drugs (1600 cm^{-1} for CR and 1399 cm^{-1} for diclofenac). An obvious drug release from the hydrogel and accumulation on the target substrate were detected for CR and diclofenac with the contact boundary shown in Figure S13. As the matrices for drug delivery, an effective release property could be observed from the developed hydrogel stamp, while its release process could also be promoted in practical body fluids with enzymes. Meanwhile, hydrogels made with natural biomacromolecules are promising candidates as a dressing material for on skin therapy. As shown in Figure 5F, the skin hydration was greatly improved after treatment with CsG-E/20B and CsG-HA hydrogels for 20 min (original skin hydration of $21.4 \pm 1.4\%$), measured with a skin moisture analyzer (BGJOY, USA). However, the skin area treated by CsG-HA exhibited a long-term hydration retention effect after 60 min with the hydration content 10% higher than those of the bare CsG-E/20B-treated ones, which can be designed for healthcare and cosmetic applications. In addition, hydrogels could serve as a soft platform for developing bioelectronics. In this work, the hydrogel was integrated with copper wires for motion sensing functions using a 4-channel recording system. As shown in Figure 5G, motions that occurred at different regions of the

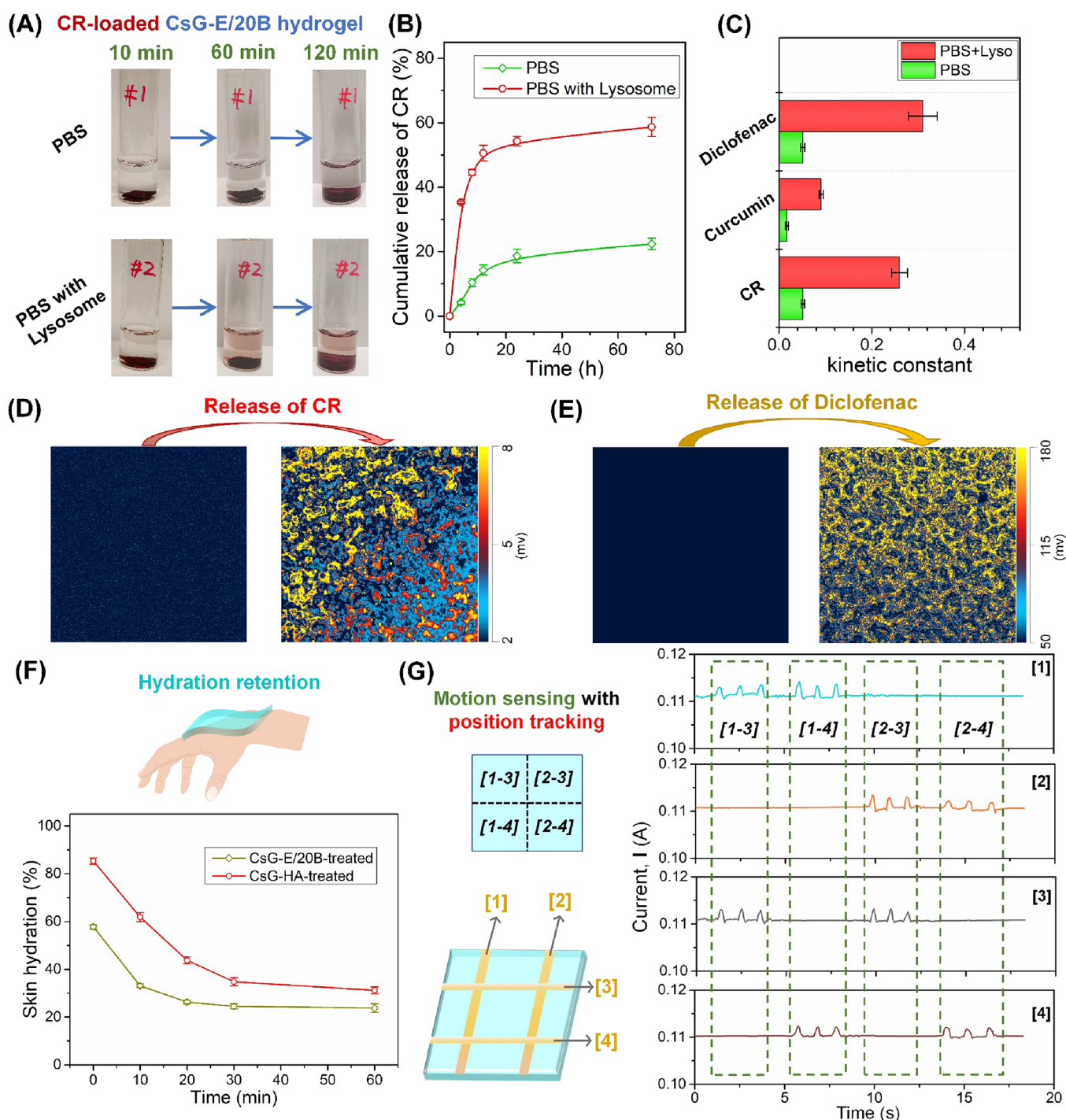


Figure 5. Drug release, skin hydration, and motion sensing functions of the hydrogels. (A) Photographs showing the release of the CR in different buffer solutions; (B) cumulative release of CR from CsG-E/20B hydrogels in PBS solution with the effect of lysosomes at 37 °C (\pm SD for $n = 3$ replicates per condition); (C) kinetic constants of 3 model drugs (i.e., CR, curcumin, and diclofenac) from CsG-E/20B hydrogels in different buffer solutions (\pm SD for $n = 3$ replicates per condition); O-PTIR mappings of target substrates before and after attachment with (D) CR-loaded and (E) diclofenac-loaded CsG-E/20B hydrogels. (F) Skin hydration after CsG-E/20B and CsG-HA hydrogel treatment (\pm SD for $n = 3$ replicates per condition). (G) Current–time curves showing the motion sensing function of the copper wire-integrated CsG-E/20B hydrogel.

hydrogels ([1,3], [2,3], [1,4], and [2,4]) could be clearly distinguished from current variation at different channels. This copper wire-embedded hydrogel demonstrated its adequate sensitivity for advanced motion sensing, and this design strategy (position tracking functions) could also be applied to other bioelectronics.^{48,49} Summarized from the above results, the hydrogels developed in this work hold great potential as a soft

platform coupling with multiple desirable functions to meet the terminal requirements in a wide range of healthcare applications.

CONCLUSIONS

In conclusion, we have demonstrated an innovative strategy of engineering asymmetric surface functionalities on a hydrogel stamp, of which the adhesive side faces the target substrates (e.g.,

tissues) and the lubrication side faces the biofluids for clinical tissue adhesion. The hydrogel stamp is prepared based on a covalently crosslinked Cs/Ct-gelatin network with a toughness of up to 40 MJ/m³ and an elastic modulus of up to 0.8 MPa, providing sufficient mechanical strength surpassing most load-bearing tissues such as the skin and muscle. The adhesive side of the hydrogel is capable of forming instant bonding (within 1 min) on the wet tissue epithelium, achieving robust adhesion strength (up to 60 kPa) through the PAA coating layer, facilitated by the surface hydration removal mechanism. On the other hand, the lubrication side, with the HA coating layer, exhibits an ultralow coefficient of friction (COF) of approximately 0.038 in biofluids. This coating layer helps reproduce the lubrication function of the original epithelium, thereby reducing the potential for wear-induced damage. By modifying both sides of the hydrogels, the surface characteristics are significantly altered, allowing the adhesives to meet the requirements of various biomedical scenarios. The hydrogel stamp also demonstrates good biocompatibility and cell affinity with MC3T3-E1 cells. Furthermore, the developed hydrogels can serve as a soft platform for enzyme-responsive drug delivery, skin hydration retention, and biosensing functions, which further broadens their applications in the field of regenerative medicine and bioelectronics. This work not only solves the long-lasting challenge of artificial epithelium-substitution materials, simultaneously supporting reliable wet tissue adhesion and reproducing surface characteristics of original tissues, but also provides a new path for converting accessible biomacromolecules to mechanically robust bioactive scaffolds that are useful in a range of biomedical applications.

METHODS

Chemicals and Materials. Carboxymethyl cellulose (Cs), chitosan (Ct, degree of deacetylation: 90%), gelatin type A, *N*-(3-dimethylaminopropyl)-*N'*-ethylcarbodiimide hydrochloride (EDC), *N*-hydroxysuccinimide (NHS), polyacrylic acid (PAA, *M_w* of 100,000), hyaluronic acid (HA), phosphate-buffered saline (pH 7.4), calcium chloride, and sodium tetraborate decahydrate were purchased from Sigma-Aldrich (Canada). The bovine muscle, porcine skin, and liver were obtained from the local grocery store. Deionized (DI) water was used in all the experiments in this work as the solution generated by a Barnstead Smart2Pure pro water purification system (Thermo Scientific).

Synthesis of CsG and CtG Hydrogels. To prepare the CsG hydrogel, 1.5 g of Cs was first dissolved in 50 mL of water (pH = 8) under stirring at 40 °C. Then, 5 g of gelatin (G) was added to the solution until a clear solution was obtained. Similarly, for the preparation of the CtG hydrogel, 1.5 g of Ct was first dissolved in 50 mL of water (pH = 4) under stirring at 40 °C followed by the addition of 5 g of G until a clear solution was obtained. Once the CsG and CtG mixture solution was prepared, it was transferred into a rectangular mold and placed in the refrigerator at 2 °C for 30 min to allow for gelation. The molded CsG and CtG hydrogels were then immersed in an EDC/NHS solution for 2 h and washed with deionized (DI) water twice for each sample. In the next step, the CsG and CtG samples were immersed in an 800 mM ammonium sulfate saline solution containing different concentrations of sodium borate, which were subsequently washed with DI water three times for each sample. The adhesion side of the hydrogel was prepared by spreading a layer of 5% PAA solution on the hydrogel followed by 30 min of air blowing to remove the surface hydration. The lubrication side of the hydrogel was prepared by spreading several drops of 10 mM CaCl₂ and 20 mM HA solution followed by 30 min of air blowing to remove the surface hydration. The final product after PAA and HA coating is referred as the hydrogel stamp in this work.

Characterization of the Hydrogels. Hydrogel samples for SEM/FTIR analysis were first quenched in liquid nitrogen and freeze-dried at

−55 °C. The freeze-dried samples were then cut carefully to obtain a smooth section for further characterization. The chemical composition of the as-prepared hydrogel was analyzed by a Fourier-transform infrared (FTIR) spectrometer (Thermo Scientific Nicolet, iS50 FT-IR). Before SEM/EDS characterization, a thin layer of gold (~14 nm) was sputtered on the hydrogel samples. The internal morphologies of the hydrogels were investigated using a field-emission scanning electron microscope (FE-SEM) (Zeiss Sigma 300 VP-FESEM, Germany) operated at a 10 keV acceleration voltage. The transmittance of the hydrogel samples was characterized by UV–vis spectroscopy at the wavelength range of 400 to 800 nm.

The viscoelastic property of the hydrogels was characterized by an AR-G2 stress-controlled rheometer (TA Instruments) using a 20 mm parallel plate configuration and a 600 μm gap. Oscillatory frequency sweep tests were performed at the range of 0.1 to 100 rad/s for both CS-GL and CT-GL hydrogels with a fixed strain of 10%. The tensile tests were conducted using an AGS-X universal tensile testing machine (Shimadzu, Japan). For the tensile tests, the rectangular hydrogel specimens were prepared with the dimension of 5 mm (length) × 2.5 mm (width) × 0.3 mm (thickness) and stretched at a constant rate of 5 mm/min.

Adhesion Tests for the Hydrogel. The lap-shear test was used to evaluate the adhesion strength of the developed CS-GL and CT-GL hydrogels. The same tensile test machine (AGS-X universal tensile tester, Shimadzu, Japan) was applied for the measurement. The substrates used in this work included plastic, wood, porcine skin, and bovine muscle. One side of the porcine skin and bovine muscle was mounted on the wood plate using the superglue (Gorilla Glue, Ohio, United States). The size of the hydrogel samples was kept at 10 mm (length) × 3 mm (width) × 0.3 mm (thickness). Meanwhile, the single-side adhesion tests were conducted by mounting the substrate and hydrogel separately to the wood plate for the measurement. Before each test, the substrates were prewetted by PBS buffer and 10 mM CaCl₂ solution. After attaching to the target substrates, a preload of ~50 kPa (weights on the contact interface of the hydrogel with substrates) was applied for a specific contact time followed by lap-shear tests. For adhesion in bovine blood, citrated bovine blood (citrate anticoagulant to blood, 1:9 volume ratio, Nanjing Yasong Biotech Co.) was used to eliminate the influence of blood coagulation to the adhesion. A stability test was conducted by covering the adhesive-attached substrate with blood-soaked medical gauze.

Biocompatibility Test. The cytotoxicity of the hydrogels against the mouse preosteoblast MC3T3-E1 cell line (subclone 4, ATCC CRL-2593) was measured with the AlamarBlue cell viability assay.^{50,51} Cells were first cultured in minimum essential medium alpha (MEM-α) media containing 10% fetal bovine serum (FBS) and 1% penicillin–streptomycin and incubated under 37 °C with 5% CO₂ and 100% humidity. Hydrogels were sterilized by UV irradiation for 30 min. Cells were then seeded on a 96-well plate at the density of 5 × 10⁴ cells/cm² (200 μL each well). After cells reached 80% confluence, the sterile hydrogels (2 mm × 2 mm) were added to the wells to incubate with the cells for 48 h; meanwhile, cells without any treatment (media only) were set as the control. After the hydrogels were removed from the wells, the media were replaced with 200 μL of 10% AlamarBlue solution (dissolved in MEM-α media, v/v) for 4 h at 37 °C (avoiding direct light). Subsequently, 150 μL of the resultant solution was transferred to an opaque 96-well plate for the detection of fluorescence signals using a Spectramax plate reader (Molecular Devices, San Jose, CA, USA); emission and excitation wavelengths were at 590 and 560 nm, respectively. Cell viability was determined by normalizing the fluorescence signal of the treatment group to the control group.

The sterile hydrogels prepared in the cytotoxicity test were also used for the biocompatibility test. Sterile hydrogels (8 mm × 8 mm) were first placed in wells on the 24-well plate followed by seeding 1 mL of medium (containing 5 × 10⁴ cells/cm² in density). The incubation lasted for 14 days with the media refreshed every 2 days. To stain cells, cells were first washed with PBS buffer 3 times followed by adding 4% formalin solution (Sigma) for fixation purposes. After 10 min of fixation, cells were washed again with PBS (3 times) and then permeabilized with 0.1% Triton-X-100 (dissolved in PBS buffer) for

another 10 min. Subsequently, cells were washed with PBS buffer (3 times) for a third time followed by the addition of 4',6-diamidino-2-phenylindole (DAPI, 10 μ M dissolved in PBS) for 10 min for staining of cell nuclei. After removing the residual DAPI in the wells, cells were washed again using PBS (3 times). Cells were then immersed in PBS and imaged using an EVOS fluorescence imaging system (Thermo Fisher Scientific, Ottawa, Canada).

Drug Delivery Performance Test. In the in vitro drug release experiments, Congo red and curcumin and diclofenac were used as the model drugs. These drugs were added into the precursor solution of the hydrogels at the concentration of 0.2 mg/mL for Congo red, 0.05 mg/mL for curcumin, and 0.1 mg/mL for diclofenac. The drug-loaded hydrogels were incubated in PBS buffers at 37 °C. At the predetermined time points, 20 μ L of the aqueous supernatant solutions was taken out and diluted to 100 times for ultraviolet–visible (UV–vis) analyses on a Thermo Evolution 300 UV–vis spectrometer. The absorbances at 510, 430, and 280 nm were recorded for Congo red, curcumin, and diclofenac samples, respectively.

The release data were fitted using the Korsmeyer–Peppas equation:⁵²

$$\frac{M^t}{M^\infty} = k \cdot t^n$$

where M^t/M^∞ is the cumulative release fraction, k is a constant incorporating characteristics of the delivery system and the drug, and n indicates the transport mechanism.

Skin Hydration and Conductivity Test. Skin hydration was measured with a skin moisture analyzer (BGJOY, USA). The skin area was first dressed by the hydrogels for 20 min and then taken for measurement after certain exposure times (0, 10, 20, 30, and 60 min) in air. The response of the copper wire-incorporated CS-GL-E/20B hydrogel to the press motion was monitored by the real-time current–time (I – t) curves with 4 channels using an electrochemical workstation (CHI920, CH Instruments, USA) with a constant voltage of 1.5 V.

Statistical Analysis. Averaged values and standard deviation (SD) were calculated from at least 3 different measurements for each entry.

■ ASSOCIATED CONTENT

SI Supporting Information

The Supporting Information is available free of charge at <https://pubs.acs.org/doi/10.1021/acs.chemmater.3c00347>.

(Video S1) Wet adhesion on the muscle (AVI)

(Video S2) Wet adhesion on the skin (AVI)

(Video S3) Wet adhesion on the liver (AVI)

UV–vis spectrum, SEM, and FTIR analysis of the hydrogels; water contact angle on the hydrogels; rheological measurements of the CtG hydrogel; cell affinity on the PVA hydrogel; O-PTIR mappings on drug-loaded-CsG hydrogels (PDF)

■ AUTHOR INFORMATION

Corresponding Author

Hongbo Zeng – Department of Chemical and Materials Engineering, University of Alberta, Edmonton, Alberta T6G 1H9, Canada; orcid.org/0000-0002-1432-5979; Phone: +1-780-492-1044; Email: hongbo.zeng@ualberta.ca; Fax: +1-780-492-2881

Authors

Mingfei Pan – School of Biomedical Engineering and Informatics, Nanjing Medical University, Nanjing 211166, People's Republic of China; Department of Chemical and Materials Engineering, University of Alberta, Edmonton, Alberta T6G 1H9, Canada; orcid.org/0000-0001-8436-2671

Tao Shui – Department of Chemical and Materials Engineering, University of Alberta, Edmonton, Alberta T6G 1H9, Canada; School of Materials Science and Engineering, Southeast University, Nanjing 211189, People's Republic of China; orcid.org/0000-0002-3691-2744

Ziqian Zhao – Department of Chemical and Materials Engineering, University of Alberta, Edmonton, Alberta T6G 1H9, Canada; orcid.org/0000-0003-3380-2803

Mei Li – School of Biomedical Engineering and Informatics, Nanjing Medical University, Nanjing 211166, People's Republic of China

Hongbing Fan – Department of Agricultural, Food and Nutritional Science, University of Alberta, Edmonton, Alberta T6G 2P5, Canada; orcid.org/0000-0003-1049-6815

Jianping Wu – Department of Agricultural, Food and Nutritional Science, University of Alberta, Edmonton, Alberta T6G 2P5, Canada; orcid.org/0000-0003-2574-5191

Complete contact information is available at:

<https://pubs.acs.org/doi/10.1021/acs.chemmater.3c00347>

Notes

The authors declare no competing financial interest.

■ ACKNOWLEDGMENTS

The authors are grateful for financial support from the Natural Sciences and Engineering Research Council of Canada (NSERC), Canada Foundation for Innovation, Canada Research Chairs Program (H.Z.).

■ REFERENCES

- (1) Wu, J.; Yuk, H.; Sarrafian, T. L.; Guo, C. F.; Griffiths, L. G.; Nabzdyk, C. S.; Zhao, X. An off-the-shelf bioadhesive patch for sutureless repair of gastrointestinal defects. *Sci. Transl. Med.* **2022**, *14*, No. eabh2857.
- (2) Liu, F.; Yang, Y.; Wan, X.; Gao, H.; Wang, Y.; Lu, J.; Xu, L.-P.; Wang, S. Space-Confinement-Enhanced Fluorescence Detection of DNA on Hydrogel Particles Array. *ACS Nano* **2022**, *16*, 6266–6273.
- (3) Lin, S.-H.; Papadakis, C. M.; Kang, J.-J.; Lin, J.-M.; Hsu, S.-h. Injectable phenolic-chitosan self-healing hydrogel with hierarchical micelle architectures and fast adhesiveness. *Chem. Mater.* **2021**, *33*, 3945–3958.
- (4) Ma, Z.; Yang, Z.; Gao, Q.; Bao, G.; Valiei, A.; Yang, F.; Huo, R.; Wang, C.; Song, G.; Ma, D.; Gao, Z. H.; Li, J. Bioinspired tough gel sheath for robust and versatile surface functionalization. *Sci. Adv.* **2021**, *7*, No. eabc3012.
- (5) Wang, W.; Zeng, Z.; Xiang, L.; Liu, C.; Diaz-Dussan, D.; Du, Z.; Asha, A. B.; Yang, W.; Peng, Y.-Y.; Pan, M.; Narain, R.; Liu, J.; Zeng, H. Injectable self-healing hydrogel via biological environment-adaptive supramolecular assembly for gastric perforation healing. *ACS Nano* **2021**, *15*, 9913–9923.
- (6) Pan, M.; Wu, M.; Shui, T.; Xiang, L.; Yang, W.; Wang, W.; Liu, X.; Wang, J.; Chen, X.-Z.; Zeng, H. Highly stretchable, elastic, antimicrobial conductive hydrogels with environment-adaptive adhesive property for health monitoring. *J. Colloid Interface Sci.* **2022**, *622*, 612–624.
- (7) Shui, T.; Pan, M.; Li, A.; Fan, H.; Wu, J.; Liu, Q.; Zeng, H. Poly(vinyl Alcohol)(PVA)-Based Hydrogel Scaffold with Isotropic Ultra-toughness Enabled by Dynamic Amine–Catechol Interactions. *Chem. Mater.* **2022**, *34*, 8613–8628.
- (8) Wu, J.; Wu, Z.; Zeng, H.; Liu, D.; Ji, Z.; Xu, X.; Jia, X.; Jiang, P.; Fan, Z.; Wang, X.; Zhou, F. Biomechanically Compatible Hydrogel Bioprosthetic Valves. *Chem. Mater.* **2022**, *34*, 6129–6141.
- (9) Jiang, P.; Lin, P.; Yang, C.; Qin, H.; Wang, X.; Zhou, F. 3D printing of dual-physical cross-linking hydrogel with ultrahigh strength and toughness. *Chem. Mater.* **2020**, *32*, 9983–9995.

- (10) Zeng, H.; Hwang, D. S.; Israelachvili, J. N.; Waite, J. H. Strong reversible Fe³⁺-mediated bridging between dopa-containing protein films in water. *Proc. Natl. Acad. Sci.* **2010**, *107*, 12850–12853.
- (11) Xiang, L.; Zhang, J.; Wang, W.; Gong, L.; Zhang, L.; Yan, B.; Zeng, H. Nanomechanics of π -cation- π interaction with implications for bio-inspired wet adhesion. *Acta Biomater.* **2020**, *117*, 294–301.
- (12) Yan, B.; He, C.; Chen, S.; Xiang, L.; Gong, L.; Gu, Y.; Zeng, H. Nanoconfining Cation- π Interactions as a Modular Strategy to Construct Injectable Self-Healing Hydrogel. *CCS Chem.* **2021**, 2903–2916.
- (13) Higaki, Y.; Kamitani, K.; Ohigashi, T.; Hayakawa, T.; Takahara, A. Exploring the mesoscopic morphology in mussel adhesive proteins by soft X-ray spectromicroscopy. *Biomacromolecules* **2021**, *22*, 1256–1260.
- (14) Pan, M.; Nguyen, K.-C. T.; Yang, W.; Liu, X.; Chen, X.-Z.; Major, P. W.; Le, L. H.; Zeng, H. Soft armour-like layer-protected hydrogels for wet tissue adhesion and biological imaging. *Chem. Eng. J.* **2022**, *434*, No. 134418.
- (15) Yan, B.; Lv, Z.; Chen, S.; Xiang, L.; Gong, L.; Xiang, J.; Fan, H.; Zeng, H. Probing Anion- π interactions between fluoroarene and carboxylate anion in aqueous solutions. *J. Colloid Interface Sci.* **2022**, *615*, 778–785.
- (16) Yang, J.; Bai, R.; Suo, Z. Topological adhesion of wet materials. *Adv. Mater.* **2018**, *30*, 1800671.
- (17) Zhang, Q.; Zhao, B.; Lin, Z.; Shi, F.; Cheng, M. Macroscopic Supramolecular Assembly of Rigid Building Blocks Facilitated by Layer-By-Layer Assembled Microgel Film. *ACS Appl. Mater. Interfaces* **2023**, *15*, 2459–2467.
- (18) Freedman, B. R.; Kuttler, A.; Beckmann, N.; Nam, S.; Kent, D.; Schuleit, M.; Ramazani, F.; Accart, N.; Rock, A.; Li, J.; Kurz, M.; Fisch, A.; Ullrich, T.; Hast, M. W.; Tinguely, Y.; Weber, E.; Mooney, D. J. Enhanced tendon healing by a tough hydrogel with an adhesive side and high drug-loading capacity. *Nat. Biomed. Eng.* **2022**, 1167–1179.
- (19) Wu, S. J.; Yuk, H.; Wu, J.; Nabzdyk, C. S.; Zhao, X. A multifunctional origami patch for minimally invasive tissue sealing. *Adv. Mater.* **2021**, *33*, 2007667.
- (20) Zhang, Y.; Ma, S.; Li, B.; Yu, B.; Lee, H.; Cai, M.; Gorb, S. N.; Zhou, F.; Liu, W. Gecko's feet-inspired self-peeling switchable dry/wet adhesive. *Chem. Mater.* **2021**, *33*, 2785–2795.
- (21) Guo, Q.; Sun, H.; Wu, X.; Yan, Z.; Tang, C.; Qin, Z.; Yao, M.; Che, P.; Yao, F.; Li, J. In situ clickable purely zwitterionic hydrogel for peritoneal adhesion prevention. *Chem. Mater.* **2020**, *32*, 6347–6357.
- (22) Tang, Z.; He, H.; Zhu, L.; Liu, Z.; Yang, J.; Qin, G.; Wu, J.; Tang, Y.; Zhang, D.; Chen, Q. A general protein unfolding-chemical coupling strategy for pure protein hydrogels with mechanically strong and multifunctional properties. *Adv. Sci.* **2022**, *9*, 2102557.
- (23) Narkar, A. R.; Barker, B.; Clisch, M.; Jiang, J.; Lee, B. P. pH responsive and oxidation resistant wet adhesive based on reversible catechol–boronate complexation. *Chem. Mater.* **2016**, *28*, 5432–5439.
- (24) Gao, Y.; Peng, K.; Mitragotri, S. Covalently Crosslinked Hydrogels via Step-Growth Reactions: Crosslinking Chemistries, Polymers, and Clinical Impact. *Adv. Mater.* **2021**, *33*, 2006362.
- (25) Shui, T.; Pan, M.; Lu, Y.; Zhang, J.; Liu, Q.; Nikrityuk, P. A.; Tang, T.; Liu, Q.; Zeng, H. High-efficiency and durable removal of water-in-heavy oil emulsions enabled by delignified and carboxylated basswood with zwitterionic nanohydrogel coatings. *J. Colloid Interface Sci.* **2022**, *612*, 445–458.
- (26) Chen, M.; Wu, Y.; Chen, B.; Tucker, A. M.; Jagota, A.; Yang, S. Fast, strong, and reversible adhesives with dynamic covalent bonds for potential use in wound dressing. *Proc. Natl. Acad. Sci.* **2022**, *119*, No. e2203074119.
- (27) Freedman, B. R.; Uzun, O.; Luna, N. M. M.; Rock, A.; Clifford, C.; Stoler, E.; Östlund-Sholars, G.; Johnson, C.; Mooney, D. J. Degradable and Removable Tough Adhesive Hydrogels. *Adv. Mater.* **2021**, *33*, 2008553.
- (28) Shariatzadeh, F. J.; Solouk, A.; Khoulanjani, S. B.; Bonakdar, S.; Mirzadeh, H. Injectable and reversible preformed cryogels based on chemically crosslinked gelatin methacrylate (GelMA) and physically crosslinked hyaluronic acid (HA) for soft tissue engineering. *Colloids Surf., B* **2021**, *203*, No. 111725.
- (29) Li, Z.; Li, S.; Yang, J.; Ha, Y.; Zhang, Q.; Zhou, X.; He, C. 3D bioprinted gelatin/gellan gum-based scaffold with double-crosslinking network for vascularized bone regeneration. *Carbohydr. Polym.* **2022**, *290*, No. 119469.
- (30) Chen, Y.; Li, K.; Zhang, S.; Qin, L.; Deng, S.; Ge, L.; Xu, L.-P.; Ma, L.; Wang, S.; Zhang, X. Bioinspired superwetable microspine chips with directional droplet transportation for biosensing. *ACS Nano* **2020**, *14*, 4654–4661.
- (31) Yuk, H.; Varela, C. E.; Nabzdyk, C. S.; Mao, X.; Padera, R. F.; Roche, E. T.; Zhao, X. Dry double-sided tape for adhesion of wet tissues and devices. *Nature* **2019**, *575*, 169–174.
- (32) Xu, R.; Zhang, Y.; Ma, S.; Ma, Z.; Yu, B.; Cai, M.; Zhou, F. A Universal Strategy for Growing a Tenacious Hydrogel Coating from a Sticky Initiation Layer. *Adv. Mater.* **2022**, *34*, 2108889.
- (33) Bannerman, A. D.; Davenport Huyer, L.; Montgomery, M.; Zhao, N.; Velikonja, C.; Bender, T. P.; Radisic, M. Elastic biomaterial scaffold with spatially varying adhesive design. *Adv. Biosyst.* **2020**, *4*, 2000046.
- (34) Lopez-Berganza, J. A.; Song, R.; Elbanna, A.; Espinosa-Marzal, R. M. Calcium carbonate with nanogranular microstructure yields enhanced toughness. *Nanoscale* **2017**, *9*, 16689–16699.
- (35) Zhang, Q.; Li, T.; Duan, A.; Dong, S.; Zhao, W.; Stang, P. J. Formation of a supramolecular polymeric adhesive via water-participant hydrogen bond formation. *J. Am. Chem. Soc.* **2019**, *141*, 8058–8063.
- (36) Bal-Ozturk, A.; Cecen, B.; Avci-Adali, M.; Topkaya, S. N.; Alarcin, E.; Yasayan, G.; Li, Y.-C. E.; Bulkurcuoglu, B.; Akpek, A.; Avci, H.; et al. Tissue adhesives: From research to clinical translation. *Nano Today* **2021**, *36*, No. 101049.
- (37) Qu, M.; Liu, H.; Yan, C.; Ma, S.; Cai, M.; Ma, Z.; Zhou, F. Layered hydrogel with controllable surface dissociation for durable lubrication. *Chem. Mater.* **2020**, *32*, 7805–7813.
- (38) Kim, A. Y.; Kim, Y.; Lee, S. H.; Yoon, Y.; Kim, W.-H.; Kweon, O.-K. Effect of gelatin on osteogenic cell sheet formation using canine adipose-derived mesenchymal stem cells. *Cell Transplant.* **2017**, *26*, 115–123.
- (39) Montgomery, M.; Ahadian, S.; Davenport Huyer, L.; Lo Rito, M.; Civitarese, R. A.; Vanderlaan, R. D.; Wu, J.; Reis, L. A.; Momen, A.; Akbari, S.; Pahnke, A.; Li, R. K.; Caldaroni, C. A.; Radisic, M. Flexible shape-memory scaffold for minimally invasive delivery of functional tissues. *Nat. Mater.* **2017**, *16*, 1038–1046.
- (40) Banik, S. M.; Pedram, K.; Wisnovsky, S.; Ahn, G.; Riley, N. M.; Bertozzi, C. R. Lysosome-targeting chimaeras for degradation of extracellular proteins. *Nature* **2020**, *584*, 291–297.
- (41) Zhang, B.; Lai, B. F. L.; Xie, R.; Davenport Huyer, L.; Montgomery, M.; Radisic, M. Microfabrication of AngioChip, a biodegradable polymer scaffold with microfluidic vasculature. *Nat. Protoc.* **2018**, *13*, 1793–1813.
- (42) Miyagi, Y.; Chiu, L. L.; Cimini, M.; Weisel, R. D.; Radisic, M.; Li, R.-K. Biodegradable collagen patch with covalently immobilized VEGF for myocardial repair. *Biomaterials* **2011**, *32*, 1280–1290.
- (43) Zamboni, F.; Wong, C. K.; Collins, M. N. Hyaluronic acid association with bacterial, fungal and viral infections: Can hyaluronic acid be used as an antimicrobial polymer for biomedical and pharmaceutical applications? *Bioact. Mater.* **2023**, *19*, 458–473.
- (44) Ahmad, N.; Wee, C. E.; Wai, L. K.; Zin, N. M.; Azmi, F. Biomimetic amphiphilic chitosan nanoparticles: Synthesis, characterization and antimicrobial activity. *Carbohydr. Polym.* **2021**, *254*, No. 117299.
- (45) Ferguson, L. T.; Hood, E. D.; Shuvaeva, T.; Shuvaev, V. V.; Basil, M. C.; Wang, Z.; Nong, J.; Ma, X.; Wu, J.; Myerson, J. W.; Marcos-Contreras, O. A.; Katzen, J.; Carl, J. M.; Morrissey, E. E.; Cantu, E.; Villa, C. H.; Mitragotri, S.; Muzykantov, V. R.; Brenner, J. S. Dual Affinity to RBCs and Target Cells (DART) Enhances Both Organ-and Cell Type-Targeting of Intravascular Nanocarriers. *ACS Nano* **2022**, *16*, 4666–4683.

- (46) Wang, C.; Wang, D.; Miao, W.; Shi, L.; Wang, S.; Tian, Y.; Jiang, L. Bioinspired ultrafast-responsive nanofluidic system for ion and molecule transport with speed control. *ACS Nano* **2020**, *14*, 12614–12620.
- (47) Zhao, Z.; Pan, M.; Qiao, C.; Xiang, L.; Liu, X.; Yang, W.; Chen, X.-Z.; Zeng, H. Bionic engineered protein coating boosting anti-biofouling in complex biological fluids. *Adv. Mater.* **2023**, 2208824.
- (48) Luo, J.; Sun, C.; Chang, B.; Jing, Y.; Li, K.; Li, Y.; Zhang, Q.; Wang, H.; Hou, C. MXene-Enabled Self-Adaptive Hydrogel Interface for Active Electroencephalogram Interactions. *ACS Nano* **2022**, *16*, 19373–19384.
- (49) Yang, M.; Chen, P.; Qu, X.; Zhang, F.; Ning, S.; Ma, L.; Yang, K.; Su, Y.; Zang, J.; Jiang, W.; Yu, T.; Dong, X.; Luo, Z. Robust Neural Interfaces with Photopatternable, Bioadhesive, and Highly Conductive Hydrogels for Stable Chronic Neuromodulation. *ACS Nano* **2023**, *17*, 885–895.
- (50) Fan, H.; Bhullar, K. S.; Wu, J. Spent hen muscle protein-derived RAS regulating peptides show antioxidant activity in vascular cells. *Antioxidants* **2021**, *10*, 290.
- (51) Esparza, Y.; Ullah, A.; Boluk, Y.; Wu, J. Preparation and characterization of thermally crosslinked poly (vinyl alcohol)/feather keratin nanofiber scaffolds. *Mater. Des.* **2017**, *133*, 1–9.
- (52) Wu, M.; Chen, J.; Huang, W.; Yan, B.; Peng, Q.; Liu, J.; Chen, L.; Zeng, H. Injectable and self-healing nanocomposite hydrogels with ultrasensitive pH-responsiveness and tunable mechanical properties: implications for controlled drug delivery. *Biomacromolecules* **2020**, *21*, 2409–2420.